A&A 585, A101 (2016)
DOI: 10.1051/0004-6361/201527292
© ESO 2015

Astronomy & Astrophysics

Global survey of star clusters in the Milky Way

V. Integrated JHK_S magnitudes and luminosity functions⋆

N. V. Kharchenko[1,2], A. E. Piskunov[1,3], E. Schilbach[1,4], S. Röser[1], and R.-D. Scholz[5]

[1] Astronomisches Rechen-Institut, Zentrum für Astronomie der Universität Heidelberg, Mönchhofstraße 12–14, 69120 Heidelberg, Germany
[2] Main Astronomical Observatory, 27 Academica Zabolotnogo Str., 03680 Kiev, Ukraine
[3] Institute of Astronomy of the Russian Acad. Sci., 48 Pyatnitskaya Str., 109017 Moscow, Russia
[4] Max-Planck-Institut für Astronomie, Königstuhl 17, 69117 Heidelberg, Germany
[5] Leibniz-Institut für Astrophysik Potsdam (AIP), An der Sternwarte 16, 14482 Potsdam, Germany
e-mail: rdscholz@aip.de

Received 1 September 2015 / Accepted 29 October 2015

ABSTRACT

Aims. In this study we determine absolute integrated magnitudes in the J, H, K_S passbands for Galactic star clusters from the Milky Way Star Clusters survey. In the wide solar neighbourhood, we derive the open cluster luminosity function (CLF) for different cluster ages.
Methods. The integrated magnitudes are based on uniform cluster membership derived from the 2MAst catalogue (a merger of the PPMXL and 2MASS) and are computed by summing up the individual luminosities of the most reliable cluster members. We discuss two different techniques of constructing the CLF, a magnitude-limited and a distance-limited approach.
Results. Absolute J, H, K_S integrated magnitudes are obtained for 3061 open clusters, and 147 globular clusters. The integrated magnitudes and colours are accurate to about 0.8 and 0.2 mag, respectively. Based on the sample of open clusters we construct the general cluster luminosity function in the solar neighbourhood in the three passbands. In each passband the CLF shows a linear part covering a range of 6 to 7 mag at the bright end. The CLFs reach their maxima at an absolute magnitude of −2 mag, then drop by one order of magnitude. During cluster evolution, the CLF changes its slope within tight, but well-defined limits. The CLF of the youngest clusters has a steep slope of about 0.4 at bright magnitudes and a quasi-flat portion for faint clusters. For the oldest population, we find a flatter function with a slope of about 0.2. The CLFs at Galactocentric radii smaller than that of the solar circle differ from those in the direction of the Galactic anti-centre. The CLF in the inner area is flatter and the cluster surface density higher than the local one. In contrast, the CLF is somewhat steeper than the local one in the outer disk, and the surface density is lower.

Key words. globular clusters: general – open clusters and associations: general – Galaxy: stellar content – galaxies: photometry – galaxies: fundamental parameters – galaxies: star clusters: general

1. Introduction

This paper continues the study of the Galactic star cluster population based on the Milky Way Star Clusters (MWSC) survey. Within this project we aim at building a comprehensive sample of star clusters of our Galaxy with well-determined parameters, which are spatially complete enough to enable an unbiased study of the cluster population. To find cluster members and to determine cluster parameters we used a combination of uniform kinematic and near-infrared (NIR) photometric data gathered from the all-sky catalogue PPMXL[1] (Röser et al. 2010). In the first paper (Kharchenko et al. 2012, hereafter Paper I), we gave an introduction to the survey and described the observational basis and the data-processing pipeline. In a subsequent paper (Kharchenko et al. 2013), we summarised the results of the full, all-sky survey carried out for a compiled list of 3006 clusters. Moreover, we recently discovered 202 new clusters at high galactic latitudes (Schmeja et al. 2014; Scholz et al. 2015). Therefore, our full sample contains 3208 star clusters: 3061 open and 147 globular clusters.

For each cluster, we determined the combined spatial-kinematic-photometric membership and a homogeneous set of basic cluster parameters (Kharchenko et al. 2013). In the present paper we derive integrated absolute magnitudes in the three 2MASS[2] (Skrutskie et al. 2006) photometric passbands J, H, K_S for all these clusters.

Within the framework of our previous project on open clusters (Kharchenko et al. 2005b,a), here referred to as COCD (Catalogue of Open Cluster Data), integrated parameters of 650 open clusters in the B, V, J, H, K_S passbands were determined and used for constructing the cluster luminosity function, referred to hereafter as CLF (Piskunov et al. 2008; Kharchenko et al. 2009). This earlier study was based on the ASCC-2.5 catalogue[3] (Kharchenko & Roeser 2009), which has a limiting magnitude of $V_{\rm lim} \approx 12$. Our present sample is larger by a factor of about 5, but because of the lack of homogeneous

⋆ The corresponding catalogue of integrated magnitudes is only available at the CDS via anonymous ftp to cdsarc.u-strasbg.fr (130.79.128.5) or via http://cdsarc.u-strasbg.fr/viz-bin/qcat?J/A+A/585/A101

[1] ftp://cdsarc.u-strasbg.fr/pub/cats/I/317

[2] ftp://cdsarc.u-strasbg.fr/pub/cats/II/246

[3] ftp://cdsarc.u-strasbg.fr/pub/cats/I/280B

all-sky optical photometry we can only determine integrated J, H, K_S magnitudes.

Luminosity functions of star clusters play an important role in studies of extragalactic populations (see e.g. Larsen 2002; de Grijs et al. 2003; Gieles et al. 2006; Anders et al. 2007; Mora et al. 2009; Whitmore et al. 2014). However, studies of the CLF in the Milky Way are more informative, since local clusters have a number of advantages over those in extragalactic systems. Among others there are a much fainter absolute magnitude limit, and ages and distances are directly determined from resolved colour-magnitude diagrams. Before the COCD survey was completed and even in the close vicinity of the Sun, the only attempt to construct the luminosity function of open clusters (van den Bergh & Lafontaine 1984) was based on a sample of 142 clusters that, according to the authors, is not complete, even within 400 pc. The basic reason was the lack of a systematic survey of integrated magnitudes of open clusters. With the COCD survey we were able to build the CLFs both for optical B, V and for J, H, K_S passbands (Piskunov et al. 2008; Kharchenko et al. 2009). Nevertheless, the COCD survey is not large enough to study possible variations of the CLFs in the space or time domains. With MWSC we have a more abundant and deeper sample, with a larger extent of the completeness area. This gives us the possibility to tackle the topic of the cluster luminosity function in more detail.

The paper has the following structure. Section 2 gives a short overview on the input data and cluster parameters obtained within the MWSC survey so far. In Sect. 3 we describe the algorithm for determining integrated magnitudes and their accuracy. In Sect. 4 we specify the approach used for constructing cluster luminosity functions and discuss the results in Sect. 5. Section 6 summarises the results.

2. Data

A reliable estimate of integrated photometric parameters of star clusters requires proper information on cluster membership and homogeneous photometric data for cluster members. Our study is based on the all-sky catalogues PPMXL (Röser et al. 2010) and 2MASS (Skrutskie et al. 2006). We used an "improved" merger of these catalogues hereafter called 2MAst (see Paper I for a description of the 2MAst construction), to verify clusters from our input list and to determine cluster parameters in the astrometric and photometric systems that are homogeneous over the whole sky.

For each of the 3208 clusters identified in the 2MAst, the membership of stars in a cluster was determined in an iterative process described in detail in Paper I. In summary, the approach is based on a series of interactive checks of the vector point diagram of proper motions (VPD), radial density profiles, magnitude-proper motion relations, and the two-colour and colour-magnitude diagrams (CMDs). The main purpose was to clean a cluster from possible fore- and background contamination and to produce a list of the most probable members to use to determine the basic cluster parameters. For each star, we expressed its cluster membership in terms of probabilities that were calculated from the location of the star in the VPD and CMDs relative to the mean proper motion of the cluster and to the cluster isochrone, respectively.

A star in the cluster area is considered to be a most probable cluster member if its kinematic and photometric membership probabilities turn out to be higher than 61%. For each cluster, we used the data on the most probable members to determine the position of the cluster centre, its apparent size, proper motion, distance, colour excess, and age. Using this membership information, we estimated the integrated magnitudes in the J, H, K_S photometric passbands for all 3208 star clusters in the MWSC survey.

Table 1. Properties of the clusters shown in Fig. 1.

MWSC	Name	$\log t$	$M_{K_S}^{\rm br}$	$(J-K_S)^{\rm br}$	$\Delta K_S^{\rm max}$
7	Blanco 1	7.75	0.257	−0.062	7.627
274	Melotte 20	7.70	−1.048	−0.147	9.866
875	ASCC 24	7.30	−3.871	−0.429	10.457
1393	NGC 2516	8.48	−7.199	1.079	14.082
1527	NGC 2632	8.92	−2.181	0.722	10.891
2403	NGC 6124	8.28	−5.012	0.656	10.924

3. Determination of integrated magnitudes and colours of star clusters

The integrated magnitude of a star cluster is computed from the sum of the luminosities of individual members, beginning with the brightest member and successively including fainter and fainter members. The integrated magnitude is assumed to be the asymptotic limit of this sum, and it can be estimated either by extrapolation (Gray 1965) or by adopting a stellar luminosity function in the cluster (Tarrab 1982).

We define the apparent $I(P)$ and the absolute $I(M_P)$ integrated magnitudes of a cluster in a photometric passband P (with P corresponding to J, H, or K_S) as

$$I(P) = -2.5 \log\left(\sum_i^N 10^{-0.4\,P_i}\right) + \delta I(P),$$

and

$$I(M_P) = I(P) - (P - M_P).$$

Here N is the number of the most probable cluster members included in the calculation, P_i the apparent magnitude of the ith member, and $(P - M_P)$ the apparent distance modulus of the cluster in the passband P. The term $\delta I(P)$ is a correction for "unseen" members, i.e. stars fainter than the limiting magnitude of the 2MAst catalogue. We introduced this correction to relate $I(P)$ and $I(M_P)$ to the same calibration interval of stellar magnitudes for all clusters of the MWSC survey. We describe this procedure in more detail below.

An intrinsic integrated colour, e.g. $I(J - K_S)_0$, is defined as the difference of absolute integrated magnitudes in the passbands J and K_S

$$I(J - K_S)_0 = I(M_J) - I(M_{K_S}).$$

Integrated magnitudes and colours were determined from the photometric data of the most probable cluster members, i.e. stars with kinematic and photometric membership probabilities higher than 61%. The integrated parameters of star clusters are primarily defined by their brightest members whereas the contribution of fainter members is rather moderate. To illustrate the change in the integrated magnitude by successively including fainter stars, we selected six clusters among those that contain members within a relatively wide magnitude range $\Delta K_S^{\rm max} = K_S^{\rm fn} - K_S^{\rm br}$ (where $K_S^{\rm br}$ and $K_S^{\rm fn}$ are the magnitudes of the brightest and faintest members, respectively). The selected clusters are listed in Table 1, together with their ages $\log t$ and

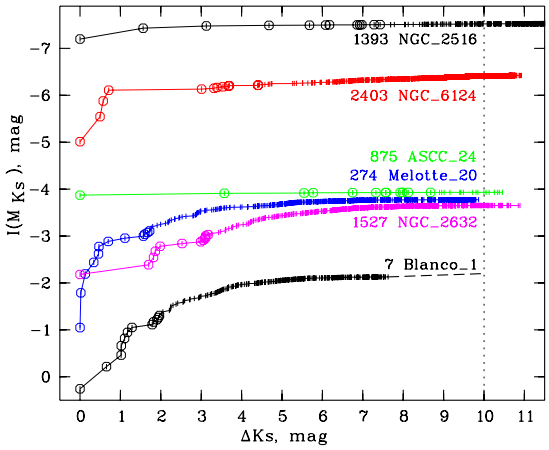

Fig. 1. Absolute integrated magnitude $I(M_{K_S})$ versus $\Delta K_S = K_S - K_S^{br}$. Individual cluster members are marked by open circles (the brightest 12 members) or by vertical bars (fainter members). The vertical dotted line at $\Delta K_S = 10$ indicates stars that are 10 mag fainter than the brightest cluster member. In the case of Blanco 1, a short dashed line shows the magnitude correction $\delta I(K_S)$ for "unseen" members.

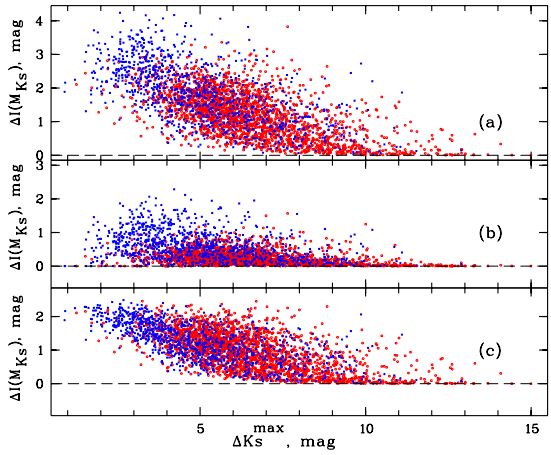

Fig. 2. Relations between different points of the clusters' luminosity profile vs. the maximum magnitude range $\Delta K_S^{max} = K_S^{fn} - K_S^{br}$. Panel **a)** shows the relation between the boundary values of the observed profile of integrated magnitudes $I^{br}(M_{K_S}) - I^{fn}(M_{K_S})$, panel **b)** the fainter part of the profile $I^{12}(M_{K_S}) - I^{fn}(M_{K_S})$, and panel **c)** its brighter part $I^{br}(M_{K_S}) - I^{12}(M_{K_S})$. Blue crosses indicate clusters with $(J - K_S)_0^{br} < 0.25$, and red circles clusters with $(J - K_S)_0^{br} \geq 0.25$.

the photometric data of the brightest members. In each cluster, the members were sorted by increasing magnitude, and the absolute integrated magnitudes $I(M_{K_S})$ were computed when fainter and fainter cluster members were included. In Fig. 1 we show the corresponding integrated magnitude profiles, i.e. the dependence of the integrated magnitude $I(M_{K_S})$ versus ΔK_S where ΔK_S is the magnitude difference between a given cluster member and the brightest cluster member. For passbands J and H, the integrated magnitude profiles are constructed analogously.

Figure 1 indicates that the accumulation of integrated brightness happens differently for the clusters and depends on several factors such as the luminosity of the brightest members, the distribution of members along the isochrone, and the presence of red giants. However, we note several features typical of the cluster luminosity profiles: a relatively fast rise in the luminosity at small ΔK_S owing to the dominant contribution of a few bright stars and a much slower increase by successively including fainter stars. As a rule, the first 10 to 12 brightest members accumulate more than half of the integrated luminosity of a cluster (Fig. 1). The integrated magnitude virtually no longer changes at $\Delta K_S > 10$.

For a quantitative description of the cluster luminosity profiles, we further introduce the following designations: the integrated magnitude $I^{fn}(M_P)$ based on all the most probable members down to the faintest magnitude in the photometric passband P, the integrated magnitude $I^{12}(M_P)$ based on the first 12 brightest members, and the absolute magnitude $I^{br}(M_P)$, or M_P^{br} of the brightest member. These values describe the accumulation of integrated brightness of a cluster at different points of the integrated magnitude profile. From the definition, $I^{fn}(M_P) < I^{12}(M_P) < I^{br}(M_P)$ evidently holds. We furthermore distinguish between clusters with and without red giants since their cumulative luminosity profiles are rather different. To make this separation, we use the colour indices of the brightest members $(J - K_S)_0^{br}$ where $(J - K_S)_0^{br} \geq 0.25$ indicates the presence of at least one red giant in a cluster, and $(J - K_S)_0^{br} < 0.25$ shows their absence. A different shape of the luminosity profiles for these two types of clusters is confirmed by Fig. 2, which shows the relations between the basic points of the clusters' luminosity profiles for the K_S passband. (For the passbands J and H, the behaviour is analogous.)

Table 2. Averaged slopes of the integrated luminosity profiles $\Delta I(P)$.

Parameter	Blue[a]	N	Red[b]	N
$\overline{\Delta I(M_J)(br,12)}$	0.140 ± 0.017	89	0.096 ± 0.020	196
$\overline{\Delta I(M_H)(br,12)}$	0.140 ± 0.024	60	0.063 ± 0.006	236
$\overline{\Delta I(M_{K_S})(br,12)}$	0.145 ± 0.033	45	0.057 ± 0.005	237
$\overline{\Delta I(M_J)(12,fn)}$	0.032 ± 0.003	89	0.024 ± 0.002	196
$\overline{\Delta I(M_H)(12,fn)}$	0.043 ± 0.005	60	0.022 ± 0.002	236
$\overline{\Delta I(M_{K_S})(12,fn)}$	0.044 ± 0.007	45	0.020 ± 0.002	237

Notes. [(a)] $I(J - K_S)_0 < 0.25$; [(b)] $I(J - K_S)_0 \geq 0.25$.

We can use the slope of the luminosity profile to characterise the contributions of different stars to the integrated magnitude of each cluster. For the 12 brightest cluster members, we compute

$$\Delta I(M_P)(\mathrm{br}, 12) = \frac{(I^{\mathrm{br}} - I^{12})}{(P^{12} - P^{\mathrm{br}})},$$

and for the remaining fainter stars

$$\Delta I(M_P)(12, \mathrm{fn}) = \frac{(I^{12} - I^{\mathrm{fn}})}{(P^{\mathrm{fn}} - P^{12})}.$$

Table 2 gives the corresponding average slopes for two types of clusters, those with and without red giants. The averages were computed only with clusters where $P^{fn} - P^{br} > 9$. Since the slopes are significantly different for these two types of clusters, the separation into "blue" $(J - K_S)_0^{br} < 0.25$ and "red" $(J - K_S)_0^{br} \geq 0.25$ clusters is justified and will be important for the estimation of the integrated magnitudes. Table 2 also gives a quantitative confirmation of the substantial contribution of the brightest members to the integrated magnitude of a cluster, whereas the contribution of fainter stars is less important: $\Delta I(M_P)(12, \mathrm{fn})$ achieves only a few hundredths per 1 mag.

We use the results of Table 2 to obtain corrections $\delta I(P)$ for "unseen" members. This correction can be substantial for clusters with small ΔP^{max} (e.g. for clusters at large distances from the

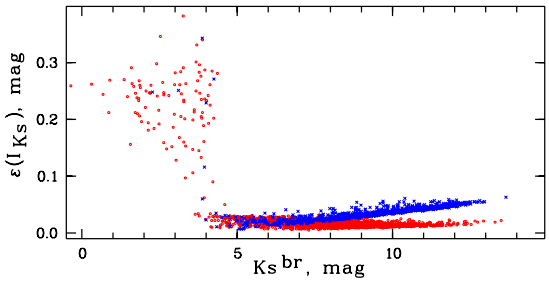

Fig. 3. rms-errors of integrated magnitudes $I(M_{K_S})$ of clusters vs. the apparent magnitudes of the brightest cluster member K_S^{br}. Blue crosses are for clusters without red giants ($(J-K_S)_0^{br} < 0.25$), and red circles for clusters with red giants ($(J-K_S)_0^{br} \geq 0.25$).

Sun). On the other hand, the integrated magnitudes $I(M_P)$ do not change significantly for $\Delta P > 10$ (see Fig. 1), so the contribution of the corresponding faint stars to the integrated magnitude can be neglected. Therefore, we chose $\Delta P = 10$ as the reference point for the correction $\delta I(P)$:

$$\delta I(P) = \overline{\Delta I(M_P)(12, \mathrm{fn})}\,(10 + M_P^{\mathrm{br}} - M_P^{\mathrm{fn}}),$$
$$I(M_P) = I^{\mathrm{fn}}(M_P) - \delta I(P).$$

For clusters with $\Delta P^{\max} > 10$, we stop the accumulation of the integrated magnitude at stars with $\Delta P = 10$.

Various factors influence the accuracy of integrated magnitudes. One of them is the measurement accuracy of the photometric data of the cluster members themselves. The corresponding rms error of an integrated magnitude can be computed straightforwardly from the photometric errors given in the catalogue via error propagation. In Fig. 3 we show the rms error of the integrated magnitudes I_{K_S} versus the magnitude of the brightest cluster member K_S^{br}. The large scatter at $K_S^{br} < 4$ results from the low measurement accuracy of bright stars in the 2MASS catalogue. Nevertheless, for the majority of clusters, the uncertainty of the integrated magnitudes due to the rms errors of the 2MASS data is relatively small. The systematic difference in the rms errors for "blue" and "red" clusters at $K_S^{br} > 4$ is caused mainly by the different accuracy of the correction $\delta I(M_{K_S})$.

Another important factor is the reliability of the membership determination. As we discussed above, the derived integrated parameters of clusters depend essentially on the photometric properties of their brightest members. To estimate the typical impact of uncertain membership, one could compare the results with alternative determinations based on other input data and/or different membership criteria from the literature. However, we did not find any publications on integrated parameters of Galactic clusters obtained in the NIR passbands. Usually, these parameters have been derived in the optical B, V passbands (see e.g. Battinelli et al. 1994; Lata et al. 2002). Within the COCD project (Kharchenko et al. 2009), we also used BV-photometry and proper motions from the ASCC-2.5 catalogue to determine cluster membership and integrated B, V parameters for 650 open clusters. The corresponding integrated J, H, K_S magnitudes were computed by adopting the membership information obtained from ASCC-2.5 data. From this point of view, we can assume that the integrated J, H, K_S parameters from the COCD and MWSC projects are nearly independent and can be used to estimate the precision of the results.

Figure 4 compares integrated magnitudes and colours in J, K_S passbands that we derived for open clusters common to the MWSC and COCD projects. Although the catalogues 2MAst

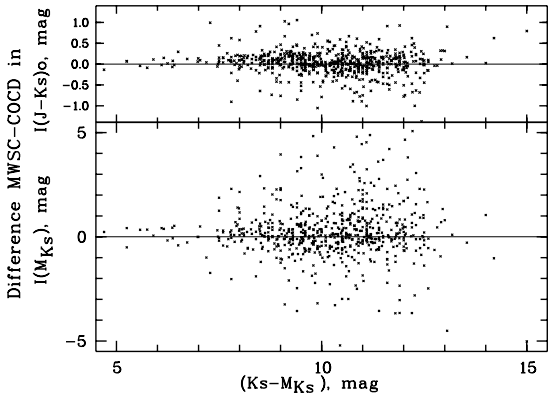

Fig. 4. Differences between integrated magnitudes (*bottom*) and colours (*top*) from the MWSC and COCD catalogues versus distance modulus of the open clusters.

Table 3. Comparison of integrated magnitudes and colours of open clusters from different sources.

Data set	N	$\Delta I(M_P)$	$\Delta I(P_1 - P_2)_0$
CM	512	-0.20 ± 0.05 (1.13)	-0.04 ± 0.01 (0.26)
CL	73	-0.26 ± 0.11 (0.93)	0.10 ± 0.04 (0.34)
CB	96	-0.28 ± 0.12 (1.17)	0.12 ± 0.03 (0.29)

Notes. CM = COCD vs. MWSC for J, K_S; CL = COCD vs. Lata et al. (2002) for B, V; CB = COCD vs. Battinelli et al. (1994) for B, V; the corresponding standard deviations are given in brackets.

and ASCC-2.5 are quite different in limiting magnitude, we observe no systematic difference in the NIR integrated magnitudes between MWSC and COCD in Fig. 4. The results of this comparison are also given in the first line of Table 3. The second and third lines show differences between integrated parameters in the B, V passbands from COCD and Lata et al. (2002) and Battinelli et al. (1994). The offset of about 0.2–0.3 mag in integrated magnitudes can probably be explained by different assumptions about the corrections for "unseen" members, whereas the uncertainties of the membership determination contribute mainly to the standard deviations given in brackets in Table 3. Assuming that all the different methods (different authors) provide the membership with similar reliability, we conclude that the MWSC integrated magnitudes are accurate to 0.7−0.8 mag.

4. Sample completeness and luminosity function construction

For statistical studies, it is essential to know how complete and representative the sample under consideration is. We already found in a preliminary analysis (Kharchenko et al. 2013) that the MWSC survey is generally complete up to a distance of 1.8 kpc from the Sun. However, the completeness depends on various parameters of clusters, primarily on their absolute brightness. Therefore, to construct an unbiased luminosity function of open clusters, one has to find a relation between absolute magnitude and completeness distance specific to a given sample.

There are, at least, two techniques for examining the completeness issue: we refer to them as a) the magnitude-limited approach and b) the distance-limited approach. Though they rely on different assumptions, both aim at determining the maximum distance from the Sun where a sample of clusters of a given integrated absolute magnitude can be rated to be complete. The

first approach is based on the assumption that the sample contains all clusters brighter than a specific apparent magnitude $\hat{I}(P)$. The second approach requires a uniform distribution of clusters on the Galactic plane, and the sample is considered to be complete up to a distance where the observed cluster density starts to deviate from some pre-specified law. The magnitude-limited approach is more economic, and it can be applied to relatively small samples, whereas the distance-limited method, being a more direct approach, requires larger samples to work effectively.

In our previous study based on the COCD survey we constructed the cluster luminosity functions using the magnitude-limited approach (Kharchenko et al. 2009). The size of the MWSC-survey enables us to apply the distance-limited approach, hence to compare both techniques.

4.1. The magnitude-limited technique

Here we briefly outline the main idea of the CLF construction based on the magnitude-limited approach. The method is described in Kharchenko et al. (2009) in more detail. We assume that our cluster sample is complete down to an integrated apparent magnitude $\hat{I}(P)$ in a photometric passband P, and we only consider clusters that are brighter than $\hat{I}(P)$. For the jth cluster of such a subsample, we can determine a completeness distance $\hat{d}_{xy,j}$ in the Galactic plane, which only depends on the completeness limit $\hat{I}(P)$, the cluster's absolute magnitude $I_j(M_P)$, and the interstellar extinction $A_{P,j}$ on the line of sight to the cluster:

$$\log \hat{d}_{xy,j} = 0.2\,(\hat{I}(P) - I_j(M_P) - A_{P,j} + 5) + \log\cos b_j, \qquad (1)$$

where b_j is the galactic latitude of the cluster. We use here the subscript j to emphasise the individual character of the derived limiting distance. With this parameter the cluster gives its individual contribution (a partial density) to the local surface density, which can be computed as $1/(\pi\hat{d}^2_{xy,j})$. Then, the cluster luminosity function ϕ is constructed as the sum of partial densities of clusters with absolute integrated magnitudes in the range $I_i(M_P)$, $I_i(M_P)+\Delta I(M_P)$ where $\Delta I(M_P)$ is a bin of the distribution

$$\phi[I_i(M_P)] = \frac{1}{\Delta I(M_P)} \sum_j^{n_i} \frac{1}{\pi\,\hat{d}^2_{xy,j}}. \qquad (2)$$

Here n_i is the number of clusters in the ith magnitude bin $I_i(M_P)$, and $\sum n_i$ is the number of clusters in the completeness subsample. The CLF constructed in such a way represents a distribution of the surface density of open clusters over integrated magnitude.

The determination of the completeness limit $\hat{I}(P)$ is a crucial point of this method. In Fig. 5 we show distributions of MWSC clusters over apparent JHK_S magnitudes and predictions of cluster counts based on a model developed by Kharchenko & Schilbach (1996) and on the data of the local cluster population derived in Piskunov et al. (2006). The approach is described in more detail in Kharchenko et al. (2009). From Fig. 5 we estimate the completeness magnitudes of the MWSC survey to be $\hat{I}(J) = 7.6$, $\hat{I}(H) = 7.0$, and $\hat{I}(K_S) = 6.8$. This is about 1.5 mag deeper than found for the COCD sample in Kharchenko et al. (2009).

The distribution of apparent magnitudes is naturally dominated by clusters of moderate luminosities, and the estimates of the completeness magnitudes are, to a certain degree, defined by these clusters. Indeed, Fig. 5 indicates that the distributions of the absolutely brightest ($I(M_{K_S}) < -6.75$) and the absolutely faintest ($I(M_{K_S}) \gtrsim -1.5$) clusters differ from the distribution of the full sample. If we adopt the same completeness magnitude for all clusters, we risk over-/under-estimating the completeness distance $\hat{d}_{xy,j}$ for absolutely brightest/faintest clusters and somehow falsifying the luminosity functions at their limits.

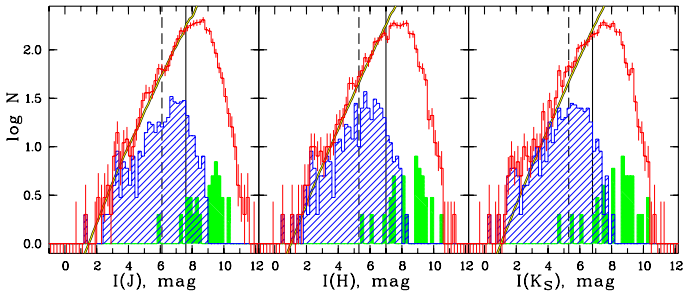

Fig. 5. Distributions of apparent integrated magnitudes for the J, H, K_S passbands of the MWSC survey. The open histograms correspond to the whole MWSC sample, the hatched histograms show the distributions of the absolutely brightest clusters ($M_{K_S} < -6.75$), whereas the filled histograms is for the distributions of the absolutely faintest clusters ($M_{K_S} > -1.5$). Bars indicate Poisson errors. Vertical solid lines indicate the adopted completeness magnitudes $\hat{I}(P)$ of the MWSC sample. The vertical dashed lines mark the completeness magnitudes estimated for the COCD sample. The double black curve shows the modelled distribution of clusters.

4.2. The distance-limited technique

This approach is based on the assumption that the surface density distribution of open clusters is, on average, uniform in the solar vicinity where the MWSC survey is actually complete (see Kharchenko et al. 2013, who determined the completeness distance of the total sample $\hat{d}_{xy,\mathrm{tot}} \approx 2$ kpc). Indeed, this expectation is confirmed by Fig. 6 (left panel), where we show how the cumulative counts of clusters increase with increasing distance from the Sun. For the total cluster sample up to a distance $d_{xy} \approx 2.2$ kpc, the number of clusters follows the law of constant surface density (see Eq. (3) below). At larger distances the counts deviate from this law indicating an increasing incompleteness of the cluster sample at $d_{xy} > 2.2$ kpc. However, the MWSC sample is large enough to carry out similar checks for subgroups of clusters in different bins of absolute integrated magnitudes. As an example, we show in Fig. 6 (left panel) the corresponding dependence for clusters with $I(M_{K_S}) = -8$–-7.

We assume that our cluster subsample is complete within a circle in the Galactic plane which is centred on the Sun and has a radius of $\hat{d}_{xy}$. If we assume further that the clusters are distributed with constant surface density Σ_0, the number of clusters N within a radius $d_{xy} \le \hat{d}_{xy}$ is simply given by

$$\log N(d_{xy}) = a + 2\,\log d_{xy}, \qquad (3)$$

with $a = \log(\pi\Sigma_0)$. This relation is indicated by black lines in Fig. 6 (left panel). At $d_{xy} \ge \hat{d}_{xy}$ the slope of the relation becomes less than 2 owing to the incompleteness of the subsample. In the following we define the completeness limit of a given cluster subsample as a distance $\hat{d}_{xy}$, where the cumulative count N_{obs} is smaller than the expected number of clusters given by Eq. (3), i.e. $\log N_{\mathrm{obs}} + \varepsilon_{\log N} < \log N(d_{xy})$ where $\varepsilon_{\log N}$ is the statistical noise. These points are indicated by large pluses in Fig. 6. Using this approach, we can determine $\hat{d}_{xy}$ for different bins of absolute magnitudes. The corresponding relation between absolute integrated magnitude of the MWSC clusters and the completeness

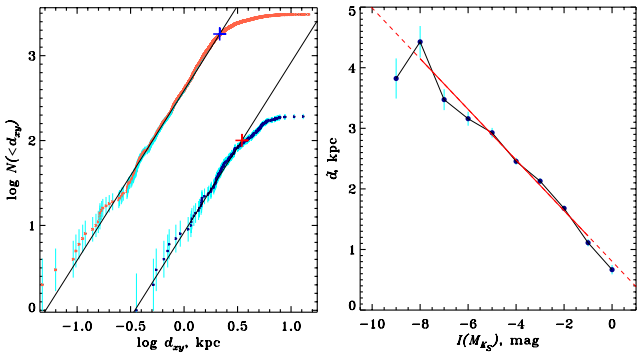

Fig. 6. Cluster counts as a function of distance in the Galactic plane d_{xy} from the Sun (*left*) and "absolute magnitude-completeness radius relation" (*right*). The counts for the whole MWSC survey are shown with small red crosses, and, as an example, counts for clusters within a magnitude bin of $I(M_{K_S}) = -8{-}{-}7$ are shown with small blue crosses. Cyan bars indicate statistical errors. The solid black lines correspond to the uniform surface density expressed by Eq. (3). The adopted completeness radii are labelled by large blue and red pluses. The *right panel* shows the completeness radii as a function of the absolute magnitude of clusters from the MWSC survey. The corresponding linear fit is indicated by a red line. The solid portion indicates where the fit is made, and the dashed segments extrapolate the fitted relation outside the fitting range.

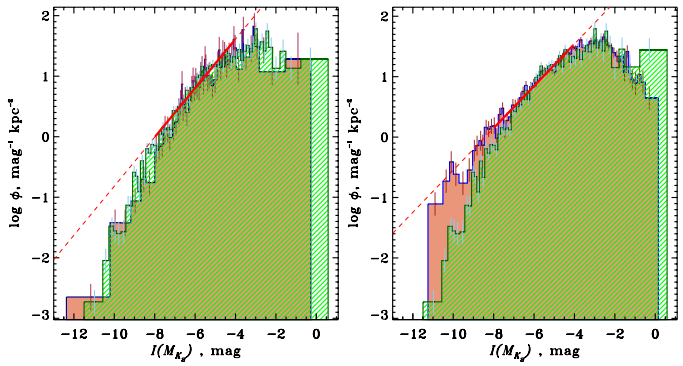

Fig. 7. Comparison of cluster luminosity functions in the K_S passband. built for different samples (MWSC and COCD) and different completeness approaches. *Left panel*: CLFs based on the magnitude-limited approach for the COCD cluster sample (red filled histogram) and for the MWSC cluster sample (green hatched histogram). *Right panel*: CLFs for the MWSC cluster sample based on two different techniques, the distance-limited approach (red filled histogram) and the magnitude-limited approach (green hatched histogram). The Poisson errors are shown with vertical bars. The thick lines mark linear fits of the MWSC CLFs in the magnitude range ($I(M_{K_S}) = -8{-}{-}4$). The extrapolation of the fits outside this magnitude range is shown by the dashed lines.

Table 4. Values of p, q-coefficients for different passbands

Band	p, kpc	ε_p	q, kpc/mag	ε_q
J	0.78	0.04	−0.52	0.02
H	0.96	0.05	−0.36	0.02
K_S	0.80	0.05	−0.42	0.02

distance is shown in the right-hand panel of Fig. 6 for the passband K_S. The relation is almost linear and can be approximated[4] well by the following equation

$$\hat{d}_{xy} = p + q\, I(M_P). \quad (4)$$

The coefficients p and q and their rms errors ε are given in Table 4.

Taking Eq. (4) into account, we compile the cluster luminosity function ϕ as

$$\phi(I_i) = \frac{1}{S(I_i)} \frac{\Delta N(I_i)}{\Delta_i I}, \quad (5)$$

where $I_i \equiv I_i(M_P)$ is the centre of the ith magnitude bin, $\Delta_i I$ is the magnitude step (generally of a variable size to ensure a minimum number of 5 clusters per magnitude bin), and $\Delta N(I_i)$ is the number of clusters within the ith magnitude bin $[I_i - \Delta_i I/2, I_i + \Delta_i I/2]$ and within the corresponding completeness circle of the surface $S(I_i) = \pi \hat{d}^2_{xy,i}$. The CLFs constructed in such a way represent a distribution of the surface density of open clusters over absolute integrated magnitude $I(M_P)$.

As Eq. (5) implies, the accuracy of the constructed CLF depends both on statistical noise and on the accuracy of the "completeness-distance-magnitude" relation (Eq. (4)). To estimate how the latter uncertainty affects the total accuracy of the CLF, we computed the contribution of this effect via the propagation of the relation uncertainty into the Poisson noise of the CLF. As expected, this contribution is small. Even for the most populated bins of $I(K_S) \approx -5{-}{-}2$, the Poisson bars are only increased by 10−20%. The contribution becomes much smaller outside this magnitude range and is insignificant in the least populated bins at the extrema of the magnitude scale. Therefore, the uncertainty of the "completeness-distance-magnitude" relation is not taken into account in the following, since it does not affect the CLF parameters and their accuracy.

4.3. Comparison of the magnitude- and distance-limited techniques

One can expect that both techniques should provide similar results for cluster luminosity functions. However, being statistical methods, they are based on different assumptions and can yield results that may be distinct in detail. We applied both approaches to the MWSC survey to analyse the influence of the methods on the resulting CLFs. Moreover, using the COCD and MWSC cluster samples, which differ not only by their size, but also by their basic photometric systems, we can test the robustness of the technique.

In the right-hand panel of Fig. 7 we compare the CLFs based on the MWSC sample, constructed with the magnitude- and distance-limited techniques. In the left-hand panel, we show the luminosity functions of the COCD and MWSC surveys constructed with the magnitude-limited technique. The MWSC sample contains 1170 clusters down to a completeness magnitude of $\hat{I}(K_S) = 6.8$ mag, whereas the COCD sample has 272 clusters down to $\hat{I}(K_S) = 5.3$ mag. Although the samples are quite different, we find a striking agreement between the CLFs based on them in the left-hand panel of Fig. 7. Also, at intermediate magnitudes $I(M_{K_S}) = -8{-}{-}4$, good agreement is found when we consider the parameters of the linear fit

$$\log \phi[I(M_{K_S})] = b + s \times I(M_{K_S}). \quad (6)$$

The slopes are $s = 0.41 \pm 0.01$ (MWSC) and 0.42 ± 0.02 (COCD), and for the absolute terms we find $b = 3.23 \pm 0.09$ and 3.28 ± 0.14, respectively.

[4] Throughout the paper we perform linear fits using a method based on optimization of χ^2-statistics (see Press et al. 1993).

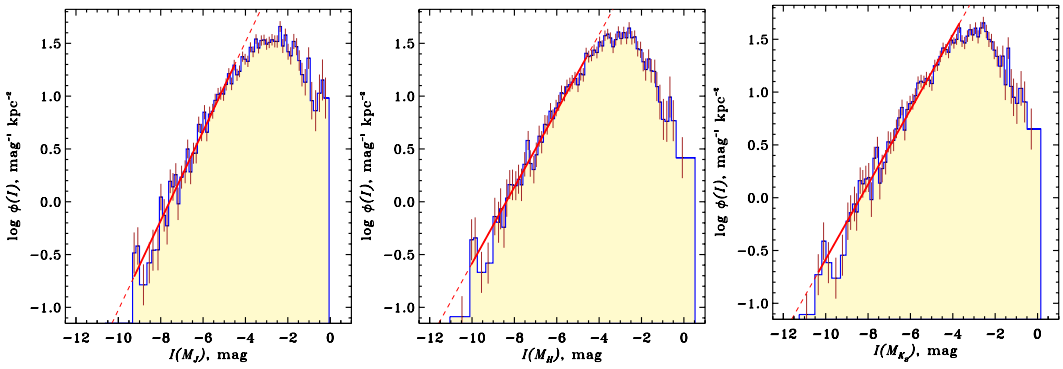

Fig. 8. General cluster luminosity functions in three NIR passbands. *Left panel* is for J, *middle panel* for H, and *right panel* for K_S. The designations are the same as in Fig. 7.

The right-hand panel shows that the two MWSC CLFs coincide well at moderate ($I(M_{K_S}) = -8.5$–-2) magnitudes. At the brightest ($I(M_{K_S}) < -8.5$) and faintest ($I(M_{K_S}) > -2$) limits, the difference between the CLFs increases and reaches a factor 50 at maximum. We explain this disagreement by a bias that is probably introduced if one adopts an apparent completeness magnitude common to all clusters, independent of their luminosities (see Sect. 4.1 and Fig. 5). As we note there, the subsample of the brightest clusters has a completeness magnitude that is about 2 mag brighter than for the full sample. In consequence, one over-estimates the completeness distance $\hat{d}_{xy,j}$ in Eq. (1) and downgrades the luminosity function. On the other hand, the completeness magnitude is under-estimated for the subsample of the absolutely faintest clusters, and the effect is reversed at the faint end of the luminosity function.

The distance-limited approach is free of this kind of biases. The corresponding luminosity function is somewhat flatter than the luminosity function based on the magnitude-limited approach, with a slope $s = 0.35 \pm 0.01$ which fits all magnitude bins brighter than $I(M_{K_S}) \approx -4$ well. The total number of clusters used for the construction of this CLF is about a factor of 2 larger than for the magnitude-limited option. This enables studies of the luminosity functions for different subsamples of clusters as a function of their age and location in the disk. For to these reasons we prefer the distance-limited approach for the CLF construction.

5. Variations in the cluster luminosity function in the time and space domains

In this section we consider possible trends of the CLFs depending on age and the location of the clusters. As a reference we use the cluster luminosity function that includes all clusters within the completeness radius determined by the distance-limited technique. Hereafter we call this CLF the general CLF (GCLF).

5.1. The general CLF

In Fig. 8 we show the GCLF constructed for the 2MASS photometric passbands. Out of 3061 clusters in the MWSC survey, more than 2000 clusters are found to be within the completeness areas. Overall, the GCLFs reveal similar features: a linear increase at brighter absolute magnitudes, which decelerates after $I(M_P) \approx -4$, and then stops at about -2.5 where the GCLFs reach their maximum. Beyond that, the GCLFs rapidly fall down and end at $I(M_P) \approx 0$, where no more cluster are in the sample. The slope of the linear portion varies a little bit and is steeper in the J-band.

Table 5. Parameters of the general cluster luminosity functions.

	J	H	K_S
N	2386	2147	2242
P_{max}	−2.35	−2.50	−2.55
s	0.42 ± 0.02	0.36 ± 0.01	0.35 ± 0.01
b	3.20 ± 0.12	3.03 ± 0.09	2.94 ± 0.06
P_{range}	−9.35–−4.5	−10.35–−4.5	−10.5–−3.6

Some key parameters of the GCLFs are given in Table 5, where N is the number of clusters used for the construction of the luminosity functions and P_{max} the magnitude of the GCLF maximum in the corresponding passband. The parameters of the regression line s and b are computed with Eq. (6), and P_{range} indicates the magnitude range where the corresponding linear fit is carried out.

Based on Fig. 8 and Table 5 we conclude that the GCLFs for the different NIR passbands cannot be distinguished dramatically from each other. Therefore, we consider only the CLFs for the K_S passband in the following.

5.2. The evolution of the CLF

The evolution of a cluster luminosity function is governed by processes accompanying the life cycle of individual clusters. In fact, two competing processes are responsible for the cluster appearance: variations in the cluster luminosity due to stellar evolution of its members and dynamical mass loss, eventually resulting in a full decay of a cluster. Whereas the dynamical evolution has a monotonic character that reduces the cluster mass, the luminosity evolves in a more complex manner. At the very early stage, during the lifetime of the most massive members, the cluster increases its luminosity. Later, the burn-out of massive stars leads to the cluster luminosity gradually decreasing. However, this process is interrupted by short flashes due to the emergence of red giants in the cluster.

Since red giants are especially bright in the NIR, these flashes play an important role in the evolution of the cluster luminosity. In the early evolutionary stages, the flashes are especially prominent, since they are caused by rare massive stars, and stochastic effects are strong. In simple terms, the bright magnitude bins of the CLFs are dominated by young and massive clusters, whereas old and/or low-mass clusters populate the faint end. Thus the CLF slope keeps information on both the cluster evolution and the cluster formation history in the Galactic disk.

To trace the evolution of the CLF with time, we divide all clusters into equal bins of $\log t$, and for each bin we build the luminosity function of clusters of the corresponding age. For a

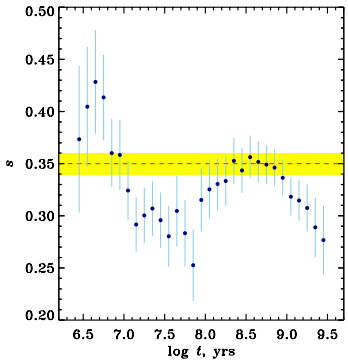

Fig. 9. Slope s of the CLF for the K_S passband versus cluster age. The rms errors of s are shown with vertical bars. The broken horizontal line indicates the slope of the general CLF, the filled strip its uncertainty.

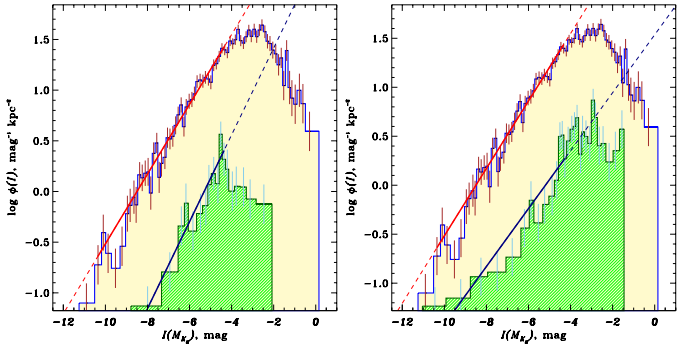

Fig. 10. CLFs for young clusters in the K_S passband. The yellow histograms show the general CLF. Green hatched histograms outline the CLFs for very young clusters ($\log t$ between 6.4 and 6.9) in the *left panel*, and for young clusters ($\log t$ from 7.2 to 7.7) in the *right panel*. The other designations are the same as in Fig. 7.

Table 6. Parameters of selected CLFs for different ages.

Age group	$\log t$	N	s	P_Q
Very young, ICLF	6.4–6.9	105	0.43 ± 0.05	0.52
Young	7.2–7.7	194	0.30 ± 0.03	0.10
Moderate	8.3–8.8	601	0.36 ± 0.02	0.47
Old	9.1–9.6	380	0.29 ± 0.03	0.26

more detailed look we use the method of the sliding window along the axis $\log t$ of width $\Delta \log t = 0.5$ and a step of 0.1 dex. In Fig. 9 we show variations in the slope of the luminosity function with cluster age. The slope shows rather complex behaviour with quasi-periodic oscillations around the GCLF slope. For a direct CLF comparison we select four subsamples of clusters of different ages. The age ranges are chosen with respect to Fig. 9: very young clusters ($\log t < 7$), young ($\log t \sim 7$–8) clusters, clusters of moderate ($\log t \sim 8$–9) ages, and old ($\log t > 9$) clusters. The corresponding CLFs are shown in Figs. 10 and 11.

Table 6 contains the CLF slopes s for each cluster subsample, and the number N of clusters used for the CLF construction. The parameter P_Q describes the goodness of the linear fit. ($P_Q < 0.1$ indicates that a given function can be hardly fitted by a single line.)

In the left-hand panel of Fig. 10, we show the CLF of the youngest group, where even massive cluster stars did not have enough time to evolve, so the bright members are still located close to the ZAMS. Therefore, we can associate their luminosity function with the initial cluster luminosity function (ICLF).

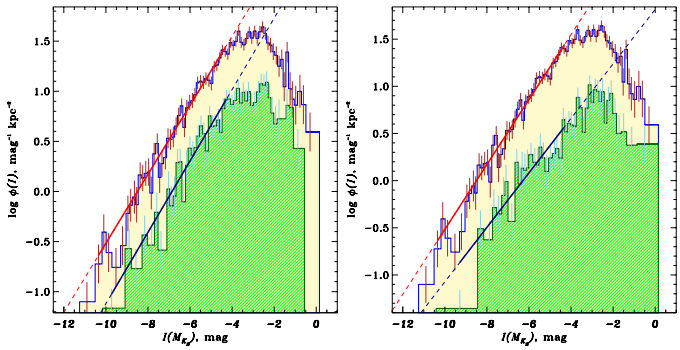

Fig. 11. CLFs for clusters of intermediate and old ages in the K_S passband. The yellow histograms show the general CLF. Green hatched histograms enclose CLFs for clusters with $\log t$ from 8.3 to 8.8 (*left panel*), and with $\log t$ between 9.1 and 9.6 (*right panel*). The other designations are the same as in Fig. 7.

Though the number of the youngest clusters is small, their CLF is fitted well ($P_Q = 0.52$) at $I(M_{K_S}) < -4.5$ by a straight line with a relatively steep slope. At fainter magnitudes the CLF drops and then slowly decreases until its faintest magnitude bin at $I(M_{K_S}) = -2$. Considering this subsample, the contribution to the surface density is the same for bright ($I(M_{K_S}) < -4.5$) clusters and for fainter clusters ($I(M_{K_S}) > -4.5$). Moreover, this proportion is kept in each age bin up to $\log t = 7$ in Fig.9.

The luminosity function of the second subsample of young clusters is shown in the right-hand panel of Fig. 10. Its slope is flatter, and the agreement with the linear power law is much worse ($P_Q = 0.10$) than in the previous case. One gets the impression that the CLF consists of two parts. The fainter one (at $I(M_{K_S}) \sim -7$–-4) is as steep as the ICLF, whereas the brighter section shows a shallower slope. Probably, this can be explained by the evolution of O-B stars. Some clusters from this age group could initially contain O-B stars that have already evolved into supergiants. This leads to an increase of the integrated luminosity of these clusters. The remaining clusters of this age range include less massive stars, therefore their integrated luminosities do not change considerably. Taken together, we observe an extension of the CLF to bright magnitude bins, whereas the CLF at intermediate magnitude ranges remains unaffected. This results in a destruction of the initial linearity of the ICLF, and a formal decrease of the slope.

In Fig. 11 we show the CLFs of older clusters. The left-hand panel corresponds to open clusters with ages typical of clusters in the solar vicinity. These clusters are old enough to contain stars of intermediate mass (down to late A stars) already evolved from the main sequence. Thus stellar evolution has an effect at integrated magnitudes down to $I(M_{K_S}) \sim 0$. Also, the considered time interval is large enough to make the effects of dynamical evolution more pronounced. This results in a cluster redistribution along the magnitude scale owing to a loss of stars, especially at the faint end of the CLF. As a consequence of stellar and dynamical evolution, we observe the steepening of the linear portion of the CLF and its extension to fainter magnitudes. Since this age group of open clusters is the most abundant, the typical slope of their CLFs (Fig. 9) is similar to that of the GCLF.

Finally, the luminosity function of the oldest clusters is shown in the right-hand panel of Fig. 11. Here we observe a further extension of the CLF to faint magnitudes, as a continuous progression of the mass-loss process making the clusters less populated and fainter. On the other hand, the brighter magnitude segment contributes again to a flattening of the CLF. This occurs

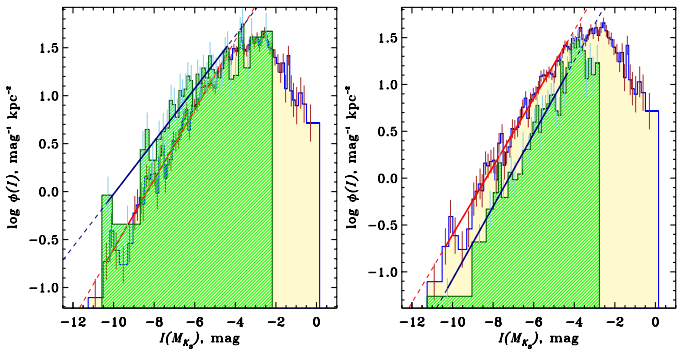

Fig. 12. Comparison of the general cluster luminosity function in K_S (yellow histograms) with the counterparts (green histograms) from the inner (*left panel*) and outer (*right panel*) disk areas. The designations are the same as in Fig. 7.

because of a higher proportion of clusters with red giants, which are quite bright in the NIR at these ages. According to Fig. 9, the CLF flattening continues with further ageing of clusters.

5.3. Variations in CLF with Galactocentric distance

In constructing CLFs in the previous sections, we assumed that the completeness distance of our cluster sample does not depend on the direction and distance from the Sun, meaning that we postulated a uniform distribution of clusters within the Galactic plane. This is justified as long as we consider some "local" CLF in an area around the position of the Sun. In this section, we compare the luminosity functions of clusters at different locations in the Galactic disk. The primary point of interest is to identify possible variations in CLFs as a function of Galactocentric distance R_G. In the following we adopt $R_G = 8.5$ kpc for the Sun.

As a first step, we built two groups of clusters: "inner" clusters ($R_G \leq 7$ kpc), and "outer" clusters ($R_G \geq 10$ kpc). We chose these selection criteria to insure a sufficient representativity of clusters of different magnitudes in each group. Following the procedure described in Sect. 4.2, we re-computed, for each group, the relation between the completeness distance and absolute integrated magnitude $I(M_{K_S})$ expressed by Eq. (4). We obtained $p = 1.09 \pm 0.08$ kpc, $q = -0.28 \pm 0.02$ kpc/mag for inner clusters and $p = 0.56 \pm 0.07$ kpc, $q = -0.57 \pm 0.02$ kpc/mag for outer clusters (see Table 4 for comparison with the general sample of clusters). For the same absolute magnitudes, we conclude that the completeness distances are smaller towards the Milky Way centre than for the outer disk. This can be explained by stronger interstellar extinction in the direction of the Galactic centre.

The corresponding CLFs are shown in Fig. 12. They are constructed with the technique described in Sect. 4.2 (see Eq. (5)) and include clusters of different ages. For the inner cluster group, the completeness area was computed as the intersection of a circle with a radius of $R_G = 7$ kpc centred on the Galactic centre, and the completeness circles centred on the Sun's position with radii determined by equation (4). For the outer cluster group, the Galactocentric radius of $R_G = 10$ kpc is used, respectively. The cluster populations we compare in Fig. 12 are therefore separated by at least 3 kpc. However, the average separation between inner and outer clusters depends on their absolute magnitude: for the faintest clusters it is slightly larger than 3 kpc, and it increases to about 6 kpc for the brightest clusters in the inner and outer groups. We note that in both panels the clusters with $I(M_{K_S}) > -2$ are missing because their completeness distances are smaller than 1.5 kpc from the Sun. The parameters of the luminosity functions are shown in Table 7. For comparison, we also include the local CLF counted between Galactocentric radii of 8.1 kpc and 8.9 kpc. The local CLF, in principle, does not differ from the GCLF, so it is not shown in Fig. 12.

Table 7. Parameters of selected CLFs for different Galactocentric distances.

Cluster group	R_G	N	s	P_Q
Inner	$\leqslant$7 kpc	221	0.27 ± 0.02	0.73
Local	8.1–8.9 kpc	530	0.35 ± 0.03	0.75
Outer	$\geqslant$10 kpc	304	0.40 ± 0.02	0.67

From Table 7 and Fig. 12 we find that the GCLF, the inner and outer CLFs differ systematically by their slopes and heights. Roughly speaking, the CLF slope gives an impression of the proportion of brightest to faintest clusters, whereas the heights show the surface density of clusters in a given range of absolute magnitudes. For the slope, we observe a radial gradient such that the slope increases with increasing R_G. To check the stability of this result, we vary the R_G limits adopted for the selection of clusters in the inner and outer groups. For the inner clusters, R_G is changed from 6.25 to 8 kpc, and for the outer clusters from 9 to 11 kpc. For both CLFs, the slopes do not change significantly, and the radial gradient for the CLF slope is kept. A shallower slope of the inner CLF indicates a higher fraction of absolutely bright clusters ($I(M_{K_S}) < -8$) in comparison to the GCLF, and this is even more significant if we compare the inner and outer CLFs. Among them, one mostly finds massive older clusters with red giants.

Furthermore, from the left-hand panel of Fig. 12, we notice a systematic over-density of clusters with $I(M_{K_S}) < -5$. In contrast, the outer CLF (right panel of Fig. 12) indicates a systematic under-density of clusters in the same magnitude range. For both samples, however, the surface density is comparable to that of the GCLF for fainter clusters ($I(M_{K_S}) > -5$). The different shapes of the inner and outer CLFs may hint at a general radial gradient of the cluster' surface density, which is decreasing with increasing R_G. At least for the bright and intermediate clusters, this seems to be a realistic trend. A possible explanation can be that the brighter (and more massive) clusters show some concentration to the Galactic centre, whereas faint clusters are distributed more smoothly in the Galactic plane. A lack of massive and older clusters in the outer disk may probably refer to a different formation history of Galactic clusters in the outer and inner disk. On the other hand, we cannot exclude the possibility that faint clusters may also have a higher surface density in the inner disk, but we are simply not able to reveal this effect owing to the relatively small completeness radii for faint clusters. As we note above, the faintest clusters are separated by about 3 kpc if we compare the inner and outer samples. The corresponding difference of Galactocentric distances is possibly not large enough to detect a potential trend of the surface density as a function of R_G for these clusters. To decide between the two intrepretations, one needs a deeper survey of photometric and astrometric data that will enable faint clusters to be identified at larger distances from the Sun and therewith to increase the completeness radii for these clusters.

6. Summary and conclusions

Integrated J, H, K_S magnitudes we determined for 3208 clusters from the MWSC survey, which consists of 3061 open

clusters and 147 globular clusters. The cluster sample covers wide ranges of absolute integrated magnitudes $I(M_{K_S}) = -11.7$–0.6 (-12.4–-5.2), ages $\log t = 6.0$–9.8 (9.8–10.1), and distances from the Sun $d = 0.1$–14.7 (2.2–82.5) kpc. (The data for globular clusters are given in brackets.)

Compared to the previous determination (Kharchenko et al. 2009), the number of open clusters with integrated magnitudes could be increased by about a factor of five. This allows us to apply different statistical methods for constructing the cluster luminosity functions. Moreover, the variety in cluster age and location in the Galactic plane gives a chance to tackle possible variations of CLFs of different cluster groups.

For the CLF construction, we applied two different methods to define cluster groups that can be considered as statistically complete samples, i.e. distance-limited and magnitude-limited approaches. Comparing them, we found that both methods provide similar CLFs within an intermediate rage of magnitudes ($I(M_{K_S}) = -7$–-2), but they disagree at the limits of the magnitude scale. We conclude that the magnitude-limited approach under-estimates the density of bright clusters and over-estimates the density of faint clusters.

Using the distance-limited method, we constructed the general cluster luminosity function in the solar neighbourhood for the three 2MASS passbands. We found that the corresponding GCLFs depend only weakly on the passband. In each passband the GCLF shows a linear portion at bright magnitude bins. At $I(M_P) \approx -4.5$ the increase slows down, and the CLF reaches the maximum at about $I(M_P) \approx -2$ and then drops down at $I(M_P) \approx 0$. The luminosity function covers a magnitude range of about 9.5 mag for J and 11 mag for H and K_S. The slope of the linear portion of the GCLF is somewhat steeper for the J magnitude than for the other two passbands.

Taking CLFs in the K_S passband as an example, we traced the evolution of the CLF. We found that the slope of the CLF varies with cluster ages in a complicated way reflecting the evolutionary state of the brightest cluster stars. Open clusters with ages $\log t < 7$ actually provide an initial cluster luminosity function (ICLF), which shows a relatively steep (with respect to the GCLF) slope of more than 0.4. The ICLF is clearly divided into two sections consisting of linear (bright) and quasi flat (faint) portions. The cluster luminosity function changes its initial shape at $\log t \sim 7$–8 and becomes flatter when the most massive stars leave the main sequence. They "extend" the bright end of the CLF, whereas the stars of intermediate masses keep their luminosities almost unchanged. Later, at ages $\log t \sim 8$–9, i.e. typical ages of "classical" open clusters, the most massive stars are burned out, whereas the evolution of the intermediate-mass stars defines the luminosity of the clusters. The slope of the CLF steepens again and the linear shape of the CLF holds for $I(M_{K_S}) < -4$. Also, the CLF extends to fainter magnitudes, partly from dynamical mass loss. Finally, in the oldest clusters ($\log t > 9$), the role of the brightest stars again increases due to more numerous red giants, and the CLF flattens again.

The increase in the cluster sample to fainter apparent magnitudes meant that the completeness area of the MWSC survey was extended compared to the COCD survey. This enabled the study of possible variations in CLFs at different Galactocentric distances in two disk areas located at about $R_G = 6$ kpc and $R_G = 11$ kpc. We found that the completeness radii are about 30% shorter towards the Galactic centre than in the anti-centre direction. Probably, this difference can be explained by a stronger extinction towards the Galactic centre. The CLF slope increases from the inner to the outer disk. This may indicate that massive clusters tend to be located in the inner disk. At least for the bright clusters, the surface density in the inner disk turns out to be higher by a factor of two than the local density, whereas it is smaller in the outer disk. However, the MWSC survey is not deep enough to investigate whether these trends are also valid for faint clusters.

Acknowledgements. This study was supported by Sonderforschungsbereich SFB 881 "The Milky Way System" (subproject B5) of the German Research Foundation (DFG). We acknowledge the use of the Simbad database, the VizieR Catalogue Service, and other services operated at the CDS, France, and the WEBDA facility, operated at the Institute for Astronomy of the University of Vienna. We thank the anonymous referee for helpful questions and comments.

References

Anders, P., Bissantz, N., Boysen, L., de Grijs, R., & Fritze-v. Alvensleben, U. 2007, MNRAS, 377, 91
Battinelli, P., Brandimarti, A., & Capuzzo-Dolcetta, R. 1994, A&AS, 104, 379
de Grijs, R., Anders, P., Bastian, N., et al. 2003, MNRAS, 343, 1285
Gieles, M., Larsen, S. S., Bastian, N., & Stein, I. T. 2006, A&A, 450, 129
Gray, D. F. 1965, AJ, 70, 362
Kharchenko, N. V., & Roeser, S. 2009, VizieR Online Data Catalog: I/280
Kharchenko, N., & Schilbach, E. 1996, Balt. Astron., 5, 337
Kharchenko, N. V., Piskunov, A. E., Röser, S., Schilbach, E., & Scholz, R.-D. 2005a, A&A, 440, 403
Kharchenko, N. V., Piskunov, A. E., Röser, S., Schilbach, E., & Scholz, R.-D. 2005b, A&A, 438, 1163
Kharchenko, N. V., Piskunov, A. E., Röser, S., et al. 2009, A&A, 504, 681
Kharchenko, N. V., Piskunov, A. E., Schilbach, E., Röser, S., & Scholz, R.-D. 2012, A&A, 543, A156
Kharchenko, N. V., Piskunov, A. E., Schilbach, E., Röser, S., & Scholz, R.-D. 2013, A&A, 558, A53
Larsen, S. S. 2002, AJ, 124, 1393
Lata, S., Pandey, A. K., Sagar, R., & Mohan, V. 2002, A&A, 388, 158
Mora, M. D., Larsen, S. S., Kissler-Patig, M., Brodie, J. P., & Richtler, T. 2009, A&A, 501, 949
Piskunov, A. E., Kharchenko, N. V., Röser, S., Schilbach, E., & Scholz, R.-D. 2006, A&A, 445, 545
Piskunov, A. E., Kharchenko, N. V., Schilbach, E., et al. 2008, A&A, 487, 557
Press, W. H., Flannery, B. P., Teukolsky, S. S., & Vetterling, W. T. 1993, Numerical Recipes (Cambridge: Cambridge Univ. Press)
Röser, S., Demleitner, M., & Schilbach, E. 2010, AJ, 139, 2440
Schmeja, S., Kharchenko, N. V., Piskunov, A. E., et al. 2014, A&A, 568, A51
Scholz, R.-D., Kharchenko, N. V., Piskunov, A. E., Röser, S., & Schilbach, E. 2015, A&A, 581, A39
Skrutskie, M. F., Cutri, R. M., Stiening, R., et al. 2006, AJ, 131, 1163
Tarrab, I. 1982, A&A, 113, 57
van den Bergh, S., & Lafontaine, A. 1984, AJ, 89, 1822
Whitmore, B. C., Chandar, R., Bowers, A. S., et al. 2014, AJ, 147, 78